

中国科学技术大学  
University of Science and Technology of China

本科毕业论文

题 目 月球磁异常与太阳风相互作用的动理学模拟

英 文 The kinetic simulation of the interaction between

题 目 the Moon's magnetic anomalies and the solar wind

院 系 地球和空间科学学院

姓 名 张子衿 学 号 PB18071571

导 师 陶鑫 教授

日 期 2022 年 6 月 26 日



## 摘要

月球缺乏一个全球性的磁层和大气层, 当其围绕地球旋转时, 它直接暴露在周围的太阳风和/或磁层等离子体中. 此前, 月球被认为只是被动的吸收周围等离子体, 其下游因为这种吸收会形成一个几乎完全的称为月球尾迹的真空; 而月球近表面空间环境主要由月球表面与环境等离子体之间的相互作用决定. 然而, 最近的空间任务揭示了月球与太阳风之间更为复杂和多样的相互作用, 例如太阳风质子的反射和偏转以及围绕月球磁异常区域 (lunar magnetic anomaly, LMA) 的“微型磁层”和无碰撞激波. 这些新的观测激发了人们对月球等离子体环境研究的新兴趣. 在本论文中, 我们研究了太阳风和月球地壳磁异常之间的相互作用. 我们使用 particle-in-cell 方法来模拟研究嵌入在月球表土中的磁偶极子与太阳风之间相互作用这一简化但典型的场景. 我们证实了在一般的太阳风条件下和月球磁异常的条件下, 磁异常的强度确实足以阻止太阳风直接撞击月球表面, 并形成一个微型磁层结构. 对微型磁层和参数影响的分析, 有助于我们深入了解行星磁结构中的多尺度动力学物理过程.

**关键词:** 月球磁异常, 太阳风相互作用

## ABSTRACT

The Moon, characterized by an absence of magnetosphere and atmosphere, sits directly exposed to the surrounding solar wind and/or magnetospheric plasma as the Moon revolved around the Earth. Therefore, the lunar space environment is mainly shaped by the interaction between the lunar surface and the impinging plasma. Previously, the Moon was thought as a passive absorber of the solar wind, forming a nearly complete void downstream called lunar wake. However, recent mission revealed a more complicated and diverse interaction between the Moon and the solar wind, such as the reflection and deflection of solar wind protons, formation of "mini-magnetospheres" and collisionless shocks around lunar magnetic anomalies (LMAs). These new observation sparks a new interest to the lunar plasma environment research.

In the present thesis, we investigate the interaction between the solar wind and lunar crustal magnetic anomalies. We use particle-in-cell simulation to study a simplified but typical scenario of the interaction between a magnetic dipolar embedded in the lunar regolith and solar wind. We confirm that LMAs may indeed be strong enough to stand off the solar wind from directly striking the lunar surface under typical solar wind conditions and form a mini-magnetosphere structure. The analysis of the miniature magnetosphere and parameter influence offers insight into kinetic multi-scale physical processes in the planetary magnetic structures.

**Key Words:** lunar magnetic anomaly, solar wind interaction, particle-in-cell

# Contents

Chapter 1	Introduction	3
1.1	Lunar plasma environment	3
1.1.1	Global Plasma Interaction with the Moon	4
1.1.2	Near-Surface Plasma Interaction	5
1.1.3	Lunar upstream region (observation of particles and waves)	6
1.2	Neutral particle environment around the Moon	8
1.3	Lunar magnetic anomaly	8
Chapter 2	Numerical method	10
2.1	Magnetohydrodynamics	10
2.2	Hybrid approach	12
2.3	Full-kinetic approach	12
2.3.1	Particle in cell method	13
2.4	Concluding remarks	15
Chapter 3	Crustal magnetic anomaly interactions	16
3.1	Observations	16
3.2	Simulation	17
3.3	Analysis	17
Chapter 4	PIC simulation of the solar wind interaction with the Lunar magnetic anomalies	21
4.1	Simulation methods	21
4.2	Mini-magnetosphere structure	24
4.3	Proton and Electron dynamics	28
4.4	Parametric analysis	30
4.4.1	The influence of the lunar surface and the magnetic dipole	32
4.4.2	The evolution time scale of the solar wind-Moon interaction	32
4.4.3	Numerical effect on the simulation	33

Chapter 5 Summary and conclusion	35
5.1 Future work	35
Bibliography	36
Appendix A Techinal caveats	43
A.1 Particle injection	43
A.2 Particle reflection at the boundary	44
Acknowledgements	45
Acknowledgements	46

## Chapter 1 Introduction

Last 20 years has witnessed a renewed interest in human exploration of the Moon: the number of related missions has exploded (Kaguya, Chang'E, Lunar Reconnaissance Orbiter, Chandrayaan, to name a few) and NASA has just launched a new program Artemis with the aim to send human back to the Moon (NASA, 2020, 2018). To successfully setting humanity on a sustainable course to the Moon, a detailed understanding of the lunar plasma environment is a must for spacecraft engineers to estimates the electromagnetic and plasmas impact on landing missions. Moreover, with no significant global magnetic field and atmosphere, the Moon represents a special class of plasma interactions with solar system bodies according to the M-B diagram (Barabash, 2012). The majority of the solar wind directly hit the lunar surface and magnetic field can not be induced due to the insulating nature of surface material. From this respective, the Moon can be considered as a passive absorber with most impinging plasma being absorbed or neutralized. However, observations from the recent missions have revealed a much more complex and fascinating Moon-plasma interaction with a variety of processes such as surface sputtering, solar wind scattering and even the formation of mini-magnetosphere. Because of the small system scales of the interaction areas compared with the large gyro-scale of heavy ions, many of the physical processes have a fundamentally kinetic features, generating unstable particles distributions and triggering plasma instabilities. The Moon, thus, provides us a natural laboratory to study these instabilities and wave-particle interactions in the special plasma regime.

In this paper, we provide an brief introduction in the area of solar wind interaction with the Moon and present a detailed simulation of the interaction between the Moon's magnetic anomalies and the solar wind. We also try to point out a few interesting observation of the simulation result and discuss future directions.

### 1.1 Lunar plasma environment

The Moon makes a complete orbit around Earth in 27 Earth days with an orbital radius of 240,000 miles (385,000km,  $\sim 60R_E$ ). By comparison, the magnetosphere of Earth extends 6 to 10 times the radius of Earth on the Sun-facing side and stretches out

into an immense magnetotail of hundreds of Earth radii on the nightside. So along its way, the Moon will pass through different regions including solar wind, bow shock, magnetosheath, the magnetotail lobes, and the plasma sheet. These regions differ in solar radiation and plasma condition and one could expect various interaction may happen between the Moon and the impinging plasma. In this thesis, we focused on the solar wind interaction with the dayside lunar surface because the Moon spends most of its time in the solar wind. We refer interesting reader to other literature (Harada, 2015) to understand the interactions of Earth's magnetotail plasma and the Moon.

The Moon makes a complete orbit around Earth in 27 Earth days with an orbital radius of 240,000 miles (385,000km,  $\sim 60R_E$ ). By comparison, the magnetosphere of Earth extends 6 to 10 times the radius of Earth on the Sun-facing side and stretches out into an immense magnetotail of hundreds of Earth radii on the nightside. So along its way, the Moon will pass through different regions including solar wind, bow shock, magnetosheath, the magnetotail lobes, and the plasma sheet. These regions differ in solar radiation and plasma condition and one could expect various interaction may happen between the Moon and the impinging plasma. In this thesis, we focused on the solar wind interaction with the dayside lunar surface because the Moon spends most of its time in the solar wind. We refer interesting reader to other literature (Harada, 2015) to understand the interactions of Earth's magnetotail plasma and the Moon.

### 1.1.1 Global Plasma Interaction with the Moon

To the first approximation, the impinging solar wind is completely absorbed by the Moon. No bow shock is observed in the upstream region (Ness et al., 1967) while a nearly complete void region is formed behind the Moon because of the removal of solar wind plasma. This downstream region is called the lunar wake first observed by Explorer missions in the 1960s. As the supersonic solar wind passes the the Moon, they begin to refill this tenuous region, generating many interesting phenomena. Enhanced magnetic fields is observed in the wake region as well as reduced magnetic field in the wake boundary. Theoretical models (Whang, 1968) have successfully explained these magnetic signatures in terms of current systems. Another characteristic feature of the lunar wake, namely ambipolar electric fields, is revealed by several spacecrafts in the 1990s. This electrostatic potential drop can be explained by charge separation

where lighter faster electrons expanding into the wake ahead of heavier slower ions. This ambipolar electric field decelerate electrons and accelerates ions in the expansion region, leading to a modified velocity distribution of the solar wind particles. In return, a wealth of electrostatic and electromagnetic waves can be observed (Nakagawa et al., 2003).

The first order approximation does not hold true above regions with strong local magnetic field. Observation revealed that the portion of reflected ions can increase up to 50% (Lue et al., 2011). In addition to that, heavier ions can be generated due to the bombardment of energetic particles through processes such as sputtering and scattering. All these ions may propagate towards the downstream regions because of their large gyro-radius, complicating the whole processes in the lunar wake. Classification of the solar wind protons have been explored by Nishino et al. (2009), and more future works can help pave our way towards a complete understanding of the global Moon-solar wind interaction.

### 1.1.2 Near-Surface Plasma Interaction

The Moon is a natural laboratory to investigate surface-plasma interaction and many fundamental physics processes like surface charging and surface weathering. This section serves as a brief introduction to the abundance of interesting phenomena happening near the surface.

#### 1. Surface charging

Surfaces of a body charges to a certain potential as observed by spacecraffts in the Earth's magnetosphere and interplanetary space. The Moon is no exception. This potential is determined by a balance between different charging currents, depending on the properties of the local plasma and radiation electromagnetic field. For a perfect conductive body, the current balance should hold globally. The Moon, however, has low enough surface conductivity (Ping et al., 2017) and this current balance (including plasma currents from electrons and ions, photoelectron currents generated by solar photons, and secondary electron emission from both electron and ion impact, see Whipple (1981)) need only hold locally for currents. In darkness, the electrical conductivity ranges from  $10^{14}$  S/m for lunar soils to  $10^9$  S/m for lunar rocks and electron thermal flux dominates, charging the surface negative to values on the order of the electron

temperature. But upon irradiation with sunlight, there is  $a > 10^6$  increase in electrical conductivity in both lunar soils and rocks and photoemission should generally provide the largest current source charging the surface to positive potentials on the order of the photoelectron temperature (a few eV). The large electrical conductivity change with visible and UV irradiation, combined with the low electrical conductivity of lunar materials, is responsible for the fact that lunar materials are readily chargeable and will remain electrically charged for long periods of time.

## 2. Photoemission

Photoemission is an especially important process on the dayside of the lunar surface. Incident photons with energies above the work function of the surface material can cause photoelectron emission. The work function of the lunar regolith was experimentally studied and determined to be 5 eV (Feuerbacher et al., 1972). Typically, the photoemission yield, defined as the number of emitted photoelectrons per incident photon, peaks at 10-20 eV, which is in the ultraviolet (UV) and extreme ultraviolet (EUV) ranges.

Photoemission dominates the sunlit-side charging environment and creates a photoelectron sheath above the lunar surface. Note that the plasma sheath may make the nearsurface plasma behave like a conductor, although the regolith material itself is insulating. These photoelectrons provide a particularly useful diagnostic tool for observations of the surface interaction, since they must pass through any magnetic gradient or potential drop above the surface before reaching the spacecraft. Given that photoelectrons should start with a relatively low characteristic temperature of a few eV, one can often determine many of the characteristics of both the magnetic and electric field configuration below the spacecraft by measuring these surface generated electrons. Using a one-dimensional particle-in-cell (PIC) code, Poppe et al. (2010) have further investigated and simulated the dusty plasma environment above the lunar surface.

### 1.1.3 Lunar upstream region (observation of particles and waves)

In the zero-order classical picture of the Moon-solar wind interaction, the Moon absorbed all the impinging plasma, having no impact on the upstream region. However, this over-simplifying assumption misses many interesting physical processes that occur around the lunar surface, especially in the LMAs regions. Recent observations from a

number of spacecrafsts revealed a much more fascinating scenario: plasma waves fill in the void of the Moon and modified particle distribution are detected in the near-lunar environment. This section serves to present a brief introduction to the various particles populations and waves observed on the upstream regions. A thorough review has been given by Harada et al. (2016). They have clarified, organized and outlined multiple categories of waves and particles as well as the properties and generation mechanisms of these waves in association with the lunar upstream particle distributions.

### 1. Upstream particles at the Moon

The moon modifies the solar wind component and its distribution function by the absorption of the ambient particles hitting the lunar surface and the generation of charged particles. These deformed distributions feature a departure from the equilibrium state, thus able to trigger plasma instabilities and plasma waves.

The most important population is the reflected ions. Saito et al. (2010) identify this population using MAgnetic field and Plasma experiment and Plasma energy Angle and Composition Experiment (MAP-PACE) on SELENE (Kaguya). These ions are observed to reflect over a wide range of angles larger than the area of magnetic enhancement, with a higher temperature and a lower bulk flow velocity than the incident ones (Saito et al., 2012). Lue et al. (2011) map the global proton fluxes and find that the fraction of deflected protons can rise to 50% (10% in average) over the large scale regions of lunar magnetic anomalies. Upward electric fields which are generated by the charge separation between ions and electrons are suggested to play an important role in reflecting the impinging ions (Jarvinen et al., 2014). This population are closely associated with lunar magnetic anomalies so we will use the term “reflected” to describe ions that do not strike the surface.

Another important population over regions with weak or no magnetic anomalies is the backscattered protons. When ambient ions bombard the lunar surface, they will collide with scattering centers in the surface material. Some may lose substantial energy and could be trapped in the surface material, whereas others will be backscattered out of the surface into space, either positively/negatively charged or as neutral particles.

### 2. Upstream waves at the Moon

A variety of classes of lunar upstream waves have been observed with frequency starting from ultra-low-frequency (0.01-0.1 Hz) moving up to high frequency Langmuir

waves ( $>10$  kHz).

## 1.2 Neutral particle environment around the Moon

Our understanding about the neutral particles around the Moon has been greatly advanced in recent years attributing to new equipments such as the energetic neutral atom (ENA) sensor onboard Chandrayaan-1. Though the solar wind mainly consists of plasma, charged particles like protons and electrons, neutral particles could be generated by the direct solar wind interaction with the lunar surface / regolith due to the absence of a global magnetosphere and atmosphere. Neutral particles are not affected by the electromagnetic field, therefore they can carry valuable information from the low altitude without distortion. From the measurement of the backscattered neutral particles, we can infer a lot about the detailed physical processes of the interaction. One important result of ENA observations is the discovery of “mini-magnetosphere” over the Crisium magnetic anomaly region (Wieser et al., 2010).

## 1.3 Lunar magnetic anomaly

Lunar magnetic anomalies which are small spatially strong magnetic fields on the Moon add another layer of complexity to the Moon-plasma interaction. LMAs are detected and measured first by magnetometers on the Apollo missions, and more recently by electron reflectometer on Lunar Prospector (Mitchell et al., 2008) and Kaguya (SELENE) (Hood et al., 2021a). These magnetic anomalies diverse in the scale and field strengths: some of these anomalies probably range up to hundred kilometers (km) in size and have surface fields up to thousand nanoTeslas (nT). But their sizes are still small compared to the lunar radius (1,737.5 kilometers) and fields at orbital altitudes are typically no more than 5 or 10 nT. Major science interests in lunar magnetic anomalies include investigating the origin of magnetic anomalies and its relation with the lunar swirls (Hood, 2021b). One possible mechanism for the formation of lunar swirls states that LMAs deflect or reflect the incident solar wind and may affect the space weathering of the lunar surface (Poppe et al., 2012).

Unlike other areas on the Moon, lunar magnetic anomalies interact with the incom-

ing solar wind in a significant manner and introduce plasma and field perturbations in the solar wind upstream region. By characterizing and mapping the reflected solar wind protons, (Lue et al., 2011) found a strong correlation between the locations of magnetic anomalies and the proton fluxes. And they estimated that up to 50 % of more of the solar wind is reflected at the most effective magnetic anomalies; 10 % as an average number over the observed magnetic anomalies. Protons reflected by lunar crustal magnetic fields have effects on both local and global lunar plasma environment (Fatemi et al., 2014).

## Chapter 2 Numerical method

Benefiting from the latest advances in high-performance computing, plasma simulation has reached a stage where it can be a highly valuable tool for comparing results with satellite observations, guiding theory and making predictions of space plasma phenomena. This chapter provides an introduction to computer simulation techniques in space plasma physics and give the context to use kinetic simulation to modelling the solar wind interactions with lunar magnetic anomalies.

Studying the evolution of charged particles, i.e. plasma, in electromagnetic fields may become complex as the particles create their own electromagnetic fields besides the external fields they are living in. Moreover, the various plasma regimes encompass a wide space of plasma parameters and plasma interactions range from microscopic to global scales. This multi-scale nature adds additional computation complexity which restrict the time and space domain of simulation domains. In space plasma communities, three popular approaches are magnetohydrodynamic (MHD), hybrid or kinetic plasma solvers. The kinetic approach is the most fundamental one, and one can derive other approach based on kinetic assumption. However, kinetic modelling is also the most computationally approach and even with present day supercomputers it needs serious consideration of the computation resources. All these plasma solvers comes with their own implicit assumptions, region of applicability, advantages and disadvantages when studying solar system plasma interactions.

### 2.1 Magnetohydrodynamics

The MHD approach represents all particle species by fluid and it describes the macroscopic low-frequency behavior of electrically conducting fluids such as plasmas under the influence of electromagnetic forces. This approach tremendously reduces computation costs and allows global modelling of the entire coupled solar wind-planet system. For this reason, it is often used to make prediction of space weather given the input of the realistic solar activity.

The simplest form of MHD is ideal MHD when the resistivity is negligible. In principle, the partial differential equations of ideal MHD and other MHD forms can be

derived from Boltzmann's equation ignoring small time scales and length scales like the Debye length or the gyro-radii of the charged particles. Here the ideal MHD equations are given for completeness, which just describe the conservation of mass, momentum and energy in fluid form together with the evolution of the magnetic field.

Continuity equation:

$$\frac{\partial \rho}{\partial t} + \nabla \cdot \rho \mathbf{u} = 0$$

Momentum equation:

$$\frac{\partial \rho \mathbf{u}}{\partial t} + \nabla \cdot (\rho \mathbf{u} \mathbf{u}) = \mathbf{J} \times \mathbf{B} - \nabla p$$

Energy equation:

$$\frac{\partial \mathcal{E}}{\partial t} + \nabla \cdot (\mathcal{E} \mathbf{u}) = -p \nabla \cdot \mathbf{u}$$

Induction equation:

$$\frac{\partial \mathbf{B}}{\partial t} + \nabla \times \mathbf{E} = 0$$

Solenoidal condition:

$$\nabla \cdot \mathbf{B} = 0$$

The current density  $\mathbf{J}$  and electric field  $\mathbf{E}$  are intermediate variables and can be expressed in function of the bulk plasma velocity  $\mathbf{u}$  and the magnetic field  $\mathbf{B}$  as follows:

$$\mathbf{J} = \nabla \times \mathbf{B} / \mu_0$$

and

$$\mathbf{E} = -\mathbf{u} \times \mathbf{B}$$

There are some underlying assumptions in the MHD models which given below. The validity of the assumptions needs to be hold or otherwise MHD models will give unphysical simulation results.

(1). The electron and ion densities are assumed equal and, hence, a quasineutrality condition. This limits the ideal MHD model to spatial scales larger than the Debye length.

(2). Electrons are much lighter than ions and are therefore often considered massless. Ions thus carry the mass and as a consequence (the electron plasma frequency and electron gyrofrequency have now zeros in their denominators) the electron temporal and

spatial scales are removed from the physical description, making the ion skin depth the viable length scale.

(3). Assuming an isotropic pressure, i.e., a collisional plasma with frequent inter-particle interactions, rather than a tensor, finite gyroradii effects are lost.

(4). When deriving the ideal MHD equation a Maxwellian distribution is assumed, or in other words, we expect a plasma close to local thermodynamic equilibrium.

## 2.2 Hybrid approach

Following MHD approaches, one nature thought is the hybrid modelling, in which the ions are treated kinetically and the electrons are still assumed to inertia-less and quasi-neutral fluid. This approach can be used to model phenomena on ion gyro-radius and inertial scales with the advantage of computation speed than the full particle simulations while gives a more vivid picture of plasma physics than magnetohydrodynamic simulations.

Hybrid models have been successfully applied to study the interaction between the solar wind and the Moon. (Jarvinen et al., 2014) suggest that electric potentials can be formed by simply decoupling the ion and electron motion without the need to introduce charge separation effect, using a 3-D quasi-neutral hybrid simulation.

However, ignoring the electron scales cannot always be justified. In Lapenta et al. (1996) paper, they compared the full kinetic and hybrid simulation in the case of contact discontinuities and implied that it is unlikely to observe contact discontinuities when electron thermal transport becomes significant in their kinetic simulation. Electron kinetics may play a important role on a larger scale, leading to a different evolution of the plasma. Winske et al. (2003) give a tutorial and review the past, present and future of the hybrid simulation of the hybrid approach with a focus on space physics, interesting readers may refer to their publication for more details.

## 2.3 Full-kinetic approach

Kinetic theory describes the most microscopic behavior of plasma. Theoretically, we can use the exact microscopic description: write down Maxwell's set of equations

and Newton's law  $F = ma$  for all the particles, calculate the forces between particles, update their positions and velocities and finally get their trajectories containing all the physical phenomena. Such a description is exact with no approximation. And one famous quote said "Give me the initial data on the particles and I will predict the future of the universe." However, in any realistic macroscopic system, the number of particles may be a terrifying number: storing the big data for something like  $10^{10}$  particles is a nightmare, not to say numerically solving their evolution. The number of operations to computer individual interactions grow quadratically with the number of particles. In short, such exact description is just infeasible in practice to simulate plasma even with advanced efficient algorithms.

Applying concepts like ensembles in statistical physics, we step into kinetic theory which describe the evolution of sampled finite-size macro-particles. Macro-particles representing a large amount of real particles average out the microscopic information in the exact theory and only interact via the averaged fields. Vlasov equation and Boltzmann equation are examples of the statistical kinetic equations. Though the precise information about individual particles is lost in this modeling, the kinetic theory still records the motion of particles and most importantly their velocity distributions. In this sense, it is still a kinetic approach. This description belongs to the type of the particle-mesh model in particle simulation as it treats forces as a field quantity and approximate it on a mesh (other type includes particle-particle method and particle-particle-particle-mesh method, see Verboncoeur (2005) for detailed explanation).

### 2.3.1 Particle in cell method

One particular method to numerically solve the partial differential equation in kinetic theory is the particle-in-cell (PIC) method where individual particles are tracked in continuous phase space in Lagrangian coordinates and moments of the distribution such as densities and currents are computed simultaneously on Eulerian mesh points. PIC methods were invented in the 1950s (Birdsall et al., 1985) and have gone a long way since then.

Basically, the PIC method includes the following procedures: integration of the equations of motion; interpolation of charge and current source terms to the field mesh; computation of the fields on mesh points; interpolation of the fields from the mesh to the

particle locations. Take the collisionless plasmas for example, the statistical equations to describe them is the Vlasov-Maxwell system of equations. Different species of particles are described by their respective distribution functions  $f_s(t, x, p)$  satisfying

$$\left( \partial_t + \frac{\mathbf{p}}{m_s \gamma} \cdot \nabla + \mathbf{F}_L \cdot \nabla_{\mathbf{p}} \right) f_s = 0$$

where  $s$  denotes a given species consisting of particles of charge  $q_s$ , mass  $m_s$ , and  $x$  and  $p$  denote the position and momentum of a phase-space element and  $\gamma$  is the (relativistic) Lorentz factor. The lorentz force particles feel is

$$\mathbf{F}_L = q_s(\mathbf{E} + \mathbf{v} \times \mathbf{B})$$

where  $\mathbf{E}, \mathbf{B}$  are the collective (macroscopic) electric and magnetic fields which still satisfy Maxwell's equations:

$$\nabla \cdot \mathbf{B} = 0$$

$$\nabla \cdot \mathbf{E} = \rho$$

$$\nabla \times \mathbf{B} = \mathbf{J} + \partial_t \mathbf{E}$$

$$\nabla \times \mathbf{E} = -\partial_t \mathbf{B}$$

To close these equations, the plasma in turn modify the collective electric and magnetic fields through their charge and current densities:

$$\rho(t, \mathbf{x}) = \sum_s q_s \int d^3 p f_s(t, \mathbf{x}, \mathbf{p})$$

$$\mathbf{J}(t, \mathbf{x}) = \sum_s q_s \int d^3 p \mathbf{v} f_s(t, \mathbf{x}, \mathbf{p})$$

Usually, the Maxwell's equations are solved using the finite difference time domain (FDTD) approach (Taflove et al., 2005) where the electromagnetic fields are discretized onto a staggered grid that allows for spatial-centering of the discretized curl operators in Maxwell's equations. And the motion of the quasie-particles are computed using a (second order) leap-frog integrator like the Boris pusher or Vay pusher for relativistic simulation (Vay, 2008).

## 2.4 Concluding remarks

In this chapter, we introduce the common numerical methods for space plasma simulation. In the next chapter, we are going to motivate our utilization of PIC plasma solver in the simulation of the Moon-solar wind interaction.

## Chapter 3 Crustal magnetic anomaly interactions

Given the small length scale and magnetic field strength of lunar crustal magnetic anomalies, one would expect their interaction with solar wind with more kinetic features. In this section, we present an overview of the observations related with LMAs, recent advances in simulation works and motivate our simulation through theory analysis.

### 3.1 Observations

Observation from various spacecraft have revealed a wealth of electromagnetic phenomena, including ion deflection and reflection of the incident solar wind, whistler and electrostatic waves, limb shocks, and steady electrostatic potentials above lunar magnetic anomalies.

Wieser et al. (2010) presented the first ENA image of a lunar magnetic anomaly, showing a clear enhancement around the crustal field and a decrease in the center. The decrease was 20%, thus not a complete void, but there could be voids present that are smaller than the ENA image resolution. Wieser et al. also observed a reduction in the ENA energy where the ENA flux was reduced. Vorburger et al. (2013) applied ENA imaging to the majority of the lunar surface, clearly observing reduction and deceleration of the solar wind at magnetic anomalies. The deceleration was also observed by orbital plasma instruments (Saito et al., 2012). Futaana et al. (2013) implemented a technique for measuring the surface potential using the observed ENA energy. These studies suggest surface potentials of 200 V, which help to deflect the protons of the solar wind from the surface.

The solar wind protons are not only deflected into the nearby regions, but some are also deflected/reflected away from the Moon (Saito et al., 2010). The reflected proton streams were observed to have temperatures of 100s eV, compared to the 10 eV of the solar wind. Reflection rates were 10% on average and were 50% or higher at the strongest magnetic anomalies.

Besides these observations, data from Kaguya and Chandrayaan suggests that in some cases (Wieser et al., 2010), Kurata et al. (2005), lunar crustal magnetic fields

may be strong enough to stand off the solar wind and generate a mini-magnetosphere shielding the surface. These mini-magnetosphere are typically identified with a density cavity structure and may be the smallest magnetosphere in the solar system.

## 3.2 Simulation

Thanks to the advance of computation power, the simulation efforts has evolved from magnetohydrodynamic to hybrid fluid / kinetic and now towards full kinetic plasma solvers. Earlier simulation have demonstrated that the interactions between lunar crustal magnetic anomalies and solar wind are highly non-adiabatic and multi-scale. The finite gyro-radius effect and charge-separation effect play a vital role in shaping the near surface plasma environment (Deca et al., 2016, 2015, 2014).

## 3.3 Analysis

The solar wind itself exhibits a fascinating structure on a range of spatial and temporal scale as it escapes the hot solar atmosphere and expands out into the space (Owens, 2020). The focus in this paper focus on the influence of the Moon, so a simplified model of undisturbed solar wind is assumed. Typical values of the solar wind parameters are as given to illustrate the key property of their interaction with solar wind: the interplanetary magnetic field (IMF) strength is 3.0 nT, the solar wind density is 5 cm<sup>-3</sup>, the solar wind speed is 400 km/s, the solar wind particles temperature is 10.0 eV (Harada et al., 2016). Based on these parameters, we can calculate the following physical quantities important in plasma physics.

In the interplanetary space, the thermal speed of protons, is of the order of 50 km/s, much slower than the solar wind bulk speed. In contrast, the thermal speed of solar wind electrons is of the order of 2000 km/s and is much higher than the bulk speed. There are almost no solar wind protons moving in the direction of the sun while a large number of electrons moving toward the sun initially. Lunar surface's absorption and magnetic reflection modifies the distribution function of the impinging solar wind, producing a loss cone structure in the electrons' velocity space (Halekas et al., 2012).

The gyroradius of solar proton in the undisturbed solar wind is of the order of

1000 km, larger than the typical length scale of lunar magnetic anomalies. On the other hand, the gyroradius of solar electrons is of the order of 1000 m. As a result, over the length scale of LMAs, the electrons in the flowing plasma are magnetized and protons (ions) are effectively unmagnetized. This bases our understanding to understand the structure of possible magnetosphere above LMA regions. As the solar wind approaches the lunar surface, the electrons are slowed, deflected and sometimes reflected by the magnetic structure. The ions on these scales, however, cannot respond as quickly as electrons to the changes in magnetic field, penetrating the magnetic barrier and bombard the lunar surfaces. This difference results in a charge separation, forming an electric field responsible for slowing and deflecting the solar wind ions. Kinetic effects become important in this interaction area.

Recent global maps of LMAs show a diverse magnetic configurations over low and high altitudes with a characteristics of elongated shapes and suggest that base-forming impacts influence the large-scale distribution of LMAs due to the impact demagnetization (Tsunakawa et al., 2015), Mitchell et al. (2008). Modelling of LMAs is a subject challenging on its own to study, here we adopt the dipole source approximation to model the LMAs. This is a reasonable assumption on central magnetic anomalies area in a small size and [Takahashi et al. (2014)](Takahashi et al., 2014) demonstrate that it will give similar result of magnetization directions of prism model. Using a simplifying assumption seems to lack the ability to reconstruct the realistic picture of the interaction. However, by isolating different physical mechanisms we could study the main processes and understand the influence of various parameters, which is impossible with observations in view of complex conditions they may encounter.

Assuming a dipolar source is located at  $r_0$  underneath parallel to the lunar surface with the dipole moment  $m$ . We first use the magnetohydrodynamics (MHD) approximation to evaluate the size of a magnetic dipole in the solar wind. The indicator here is the the pressure equilibrium point  $L$  as measured from the dipole center. In the equilibrium point, the dynamic pressure of the impinging solar wind is balanced by the local magnetic pressure of the plasma flow. In regions below the point, particle dynamics are significantly influenced by the local crustal magnetic field and the lunar surface, whereas in regions above the solar wind are disturbed by the reflected particles and waves that propagated upstream.

$$L = \left( \frac{\mu_0 M_d^2}{16\pi^2 N_0 m_i V_{\text{flow}}^2} \right)^{\frac{1}{6}}$$

For typical value  $M_d = 2 \times 10^{13} A \cdot m^2$ ,  $V_{\text{flow}} = 400 \text{ km/s}$ ,  $N_0 = 5 \text{ cm}^{-3}$ , this  $L$  corresponds to a value of 37 km, equivalent to  $0.35 d_i$  (ion inertial length) or  $0.25 r_{g, \text{proton}}$  (ion gyro-radius under the quiet solar wind condition)

However, this doesn't necessarily lead to the formation of an obstacle boundary. Especially in the case of lunar crustal magnetic anomalies, the incoming protons have gyro-radii comparable to the scale of the magnetic obstacle, they may not manage to turn around before they have flown past the obstacle, or impacted the lunar surface above the source of the magnetic field. In such a case, no magnetopause forms. So simulation has to be performed to check the existence of the barrier structure.

Greenstadt study the formation condition of a magnetosphere by magnetic fields of scale sizes comparable to the proton gyroradius and submagnetospheric interactions (in which a magnetosphere does not fully form) when considering the solar wind interaction with magnetized asteroids. They present three conditions required for the formation of a mini-magnetosphere that successfully stands-off the solar wind: (1) The magnetic field must be strong enough from a pressure-balance point-of-view. (2) The magnetopause distance from the surface must be greater than the solar wind stopping distance, i.e., the vertical distance required to turn-around the solar wind plasma. (3) The lateral (horizontal) scale size of the magnetic obstacle must be large enough to exclude edge-effects. If these criteria are not met, the solar wind will fill-in the crustal field and be deflected but not creating a proper void. Nevertheless, such an interaction would create various electromagnetic noise. If the solar wind deceleration is large enough, a magnetosonic shock would form even without a void region. Whistler waves would also arise from the disturbance of the solar wind, possibly creating a standing whistler wave.

Back to the Moon, observations and simulations work suggest that a submagnetospheric type of interaction is most plausible, for most of the lunar magnetic anomalies, most of the time. However, in some cases, or perhaps commonly but on small scales, mini-magnetosphere may form. Lunar albedo swirls (bright features on the lunar surface at strong magnetic anomalies) may be indicative of small plasma voids, where

surface weathering is reduced (Garrick-Bethell et al., 2011).

## Chapter 4 PIC simulation of the solar wind interaction with the Lunar magnetic anomalies

We have carried extensive trial-and-error simulations. With all the physical parameters based on their typical values (no compromise for computation speed), we confirm once again (Deca et al., 2015; Bamford et al., 2016) that it is true for LMAs to stand off the solar wind and generate a mini-magnetosphere. After an introduction to our simulation method (including the code implementation and numerical choices in detail), we present the formation process of the mini-magnetosphere in our simulation. The next section focuses on the particle dynamics (electrons and protons). And we end this chapter with a analysis of parameters that have never explored before.

### 4.1 Simulation methods

Various electromagnetic / electrostatic particle-in-cell codes have been applied to study the solar wind interaction with the Lunar magnetic anomalies, including iPIC3D (Deca et al., 2021); Deca et al. (2015), OSIRIS (Bamford et al., 2016) and HYBES (Dyadechkin et al., 2015).

The iPIC3D is an open-source C++ and MPI code developed by Markidis et al. (2010) ten years ago originally for magnetic reconnection research. Utilizing implicit discretization of the Maxwell's and particle motion equations, the code has the advantage to retain the numerical stability over explicit method codes, thus allowing simulation with longer time step and larger grid spacing. However, the current implementation of iPIC3D has considerable load imbalance problems, preventing it scaling to large simulation. What's more, at the time of the code development, standards like openPMD (Open Standard for Particle-Mesh Data Files) and PICMI (Particle-In-Cell Modeling Interface) have not yet been proposed. The code, therefore, lacks the consistency and agility to take advantage of progress in hardware like GPU devices, develop advanced features like mesh refinement and use new numerical schemas. Embarrassingly, the iPIC3D code even failed to compile with most recent version of gcc.

The OSIRIS code which is a closed source code with a proprietary licence and the

HYBes code which is an electrostatic simulation code are neither suitable for our case.

In this work, we use the open source code WarpX (Vay et al., 2018) and Smilei (Derouillat et al., 2018). Leaded by Lawrence Berkeley National Laboratory, WarpX is a successor and full reimplementation of Warp code in modern C++ with a focus on plasma wakefield accelerator design. Smilei code, on the other hand, is a collaborative code co-developed by physicists and HPC experts, leaded by Maison de la Simulation laboratory. They are both advanced electromagnetic particle-in-cell code developed in recent years to meet the exascale challenge and they contains many physics modules to applies to a wide range of studies. Detailed documentations and codes implementation can be found on their website. Here I just list a few features of these codes that is important in our study.

(1). Load balancing: by decomposing the whole simulation domain into independent sub-domains (called grids in WarpX and patches in Smilei), the codes can handle massive parallelization and and achieve dynamic load balancing by transfering subdomains to different computing units (MPI processes).

(2). Particle injection & open boundary conditions: in the case of modeling solar wind interaction with the Moon, solar wind particles are injected into the simulation continuously and absorbed (removed) when they encoutner the Moon surface. Open boundaries may approximate the realistic interaction on the surface while reflective or periodic boundary condition may introduce unphysical phenomena and influence the whole evolution of the simulation as demonstrated later in our study.

(3). External fields: to describe the charged particles' dynamics in lunar magnetic anomalies regions, a given electromagnetic field representing the LMAs configuration is required to push the particles. And it is worth further research whether this preconfigured electromagnetic field needs to participate in the Maxwell solver or not. Deca et al. (2015) argued that the most stable evolution for the LMA problem are obtained under “fixed” field BCs conditions where the fields E and B are fixed to their initial value. However, such boundaries conditions are in contradiction of the exact solution of Maxwell’s equation, making the simulation not self-consistent. One of the most important advantages for PIC method is its self-consistency. In our study, we found that this setting can have much bigger influence in simulations with a realistic plasma parameter than previously thought by Deca et al. (2015).

As discussed in the earlier section, modeling the LMA field from observations is a challenge itself. Our work focus on the general mechanism between LMA and solar wind, thus we simplify our simulation to use a dipole model representing lunar crustal magnetic field, which is a good approximation in small-scale anomaly areas. Note, Deca et al. (2021) use real observation data of magnetic field from the Kaguya and Lunar Prospector missions as input to study the plasma environment near the Reiner Gamma anomaly and their results are consistent with the solar wind standoff model. Our PIC simulation incorporate an external dipole magnetic field component

$$\mathbf{B}_m(\mathbf{r}) = \frac{\mu_0}{4\pi} \left( \frac{3(\mathbf{m} \cdot (\mathbf{r} - \mathbf{r}_0))(\mathbf{r} - \mathbf{r}_0)}{(r - r_0)^5} - \frac{\mathbf{m}}{(r - r_0)^3} \right)$$

This dipole magnetic field is superimposed on the plasma electromagnetic field. This constant field can be initialized at first as a component of the whole self-consistent magnetic field, or can be directly applied to push the particles with no participation in the PIC's Maxwell solver. Though this latter setting makes the simulation not self-consistent, it is useful to describe charged particles' dynamics in a given electromagnetic field. And our simulation demonstrate no obvious dispartion of these two options. On the solar wind incident side, the dipole magnetic fields become very weak compared to the interplanetary magnetic field. On the lunar surface, the situation reverse and the strong local magnetic fields have a dominant effect on the motion of the solar wind.

In our simulation, the interplanetary magnetic field direction is opposite to the dipole magnetic field along the line  $y = 0, z = 0$ . This setting creating a zero-point in the total magnetic field configuration at 0.8 di above the surface.

We also adopt an isothermal solar wind plasma model as the injection species of the simulation. Their bulk velocity, density and temperature are in the regime of typical solar wind conditions. And the proton-to-electron mass ratio used in the simulation is the realistic value of  $m_{proton}/m_{electron} = 1836$

For reference purpose following physical and numerical parameters are used throughout all our simulations: the solar wind density is set as  $n_{solar} = 5\text{cm}^{-3}$ , corresponding to an ion inertial length  $d_i = 100\text{km}$ ; the protons and electrons share a same temperatures of  $T_{sw} = T_i = T_e = 35\text{eV}$  and a bulk velocity speed  $v_{sw} = 400\text{km} \cdot \text{s}^{-1}$ .

Boundary conditions have a significant impact on the simulation results. Imple-

menting an universal open boundary condition satisfying any the physical condition are unfortunately impractical and impossible. Our simulation use the perfectly matched layer (PML) in all the simulation boundaries. This boundary is commonly used to simulate problems with open boundaries, especially in the FDTD and FE methods. It actes as a absorber for wave equations, well designed so that waves incident upon the PML do not reflect at the interface. Other open boundaries includes silver-muller for injecting electromagnetic field and ramp condition for the spectral solver in cylindrical geometry. For our work, we do not need to inject other electromagnetic field besides the interplanetary magnetic field and the geometry shows no favors for cylindrical shape. Therefore, we adopt the PML boundary condition, though using silver-muller boundary condition may possibly help accelerate the computation speed.

Computation code often benefits when physical quantities typically having a wide range of magnitudes, are scaled (close) to order 1. WarpX and Smilei PIC code is no exception. Maxwell's electromagnetic equations and motion equations of individual quasi-particles (Vlasov's equations) take the form under nature units while other quantities are normalized to reference quantities such as the speed of light for velocity, the elementary charge for charge and the electron mass for mass. So PIC codes only handle dimensionless variables. Besides the benefit in numerical stability and computational speed, the normalized simulation result can be applied to various physical systems, as long as the dimensionless variables are identical.

## 4.2 Mini-magnetosphere structure

Figure 4.1, 4.2 shows the density evolution of electrons and protons as the solar wind plasma impacts a localized crustal magnetic field structure. We also draw the net charge density (Figure 4.3) which has been converted to the unit of number density (in other words, proton density minus electron number) for comparison with the particle density. Non-zero net density can be clearly identified in Figure 4.3 after the simulation begins and the plasma comes into a neutral balance after the formation of the mini-magnetosphere.

As the solar wind impinges towards the lunar surface, both the proton and electron populations drift perpendicular to the magnetic field: some are deflected toward the

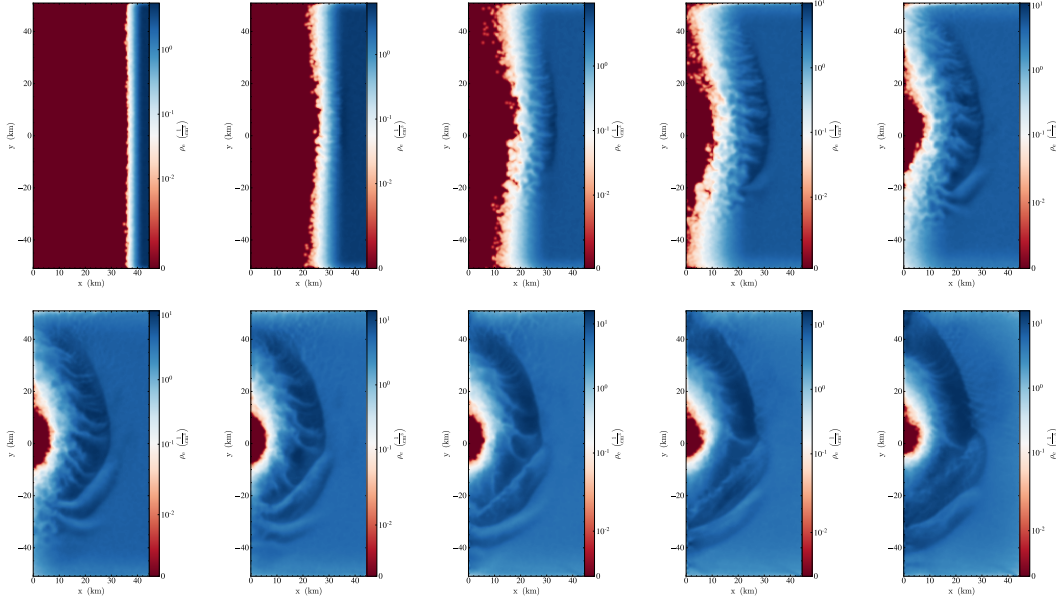


Figure 4.1 Electron number density

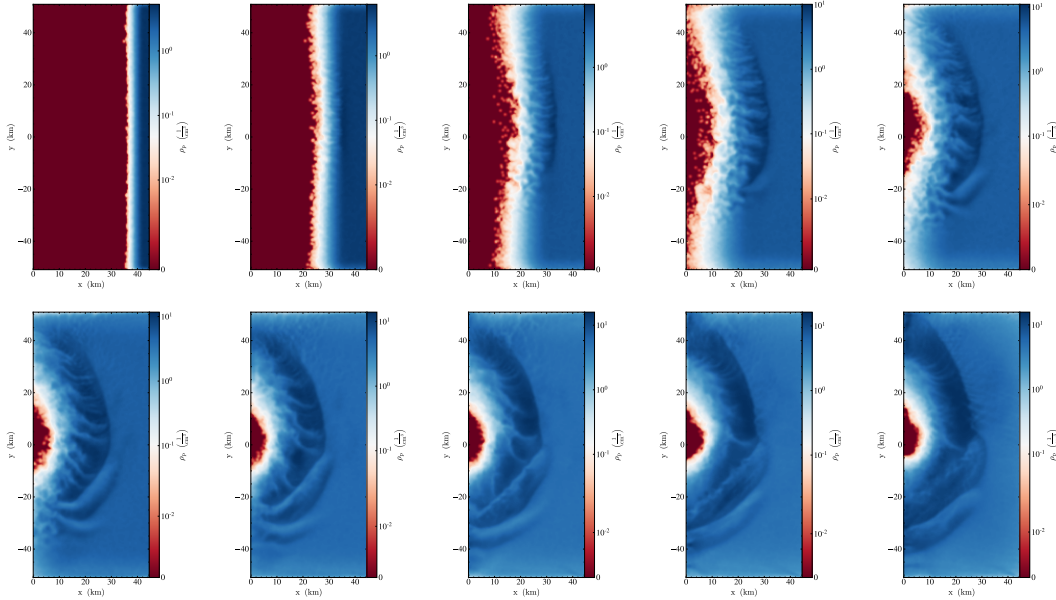


Figure 4.2 Proton number density

cusp regions of the magnetic dipole and some are reflected upstream. A density cavity is observed in the simulation box, surrounded by a higher density halo. This result is consistent with simulations performed by Deca et al. (2015) and Bamford et al. (2016). This structure has the similar effect of magnetosphere in affecting charged particles, and it is called mini-magnetosphere (Saito et al., 2012), Lin et al. (1998). This small-scale high density region is formed because the solar wind particles are temporarily packed against the dipole field. The halo has its highest point about 25 km ( $0.25 d_i$ ) above the lunar surface, has a thickness about 10 km ( $0.1 d_i$ ) and has a maximum density

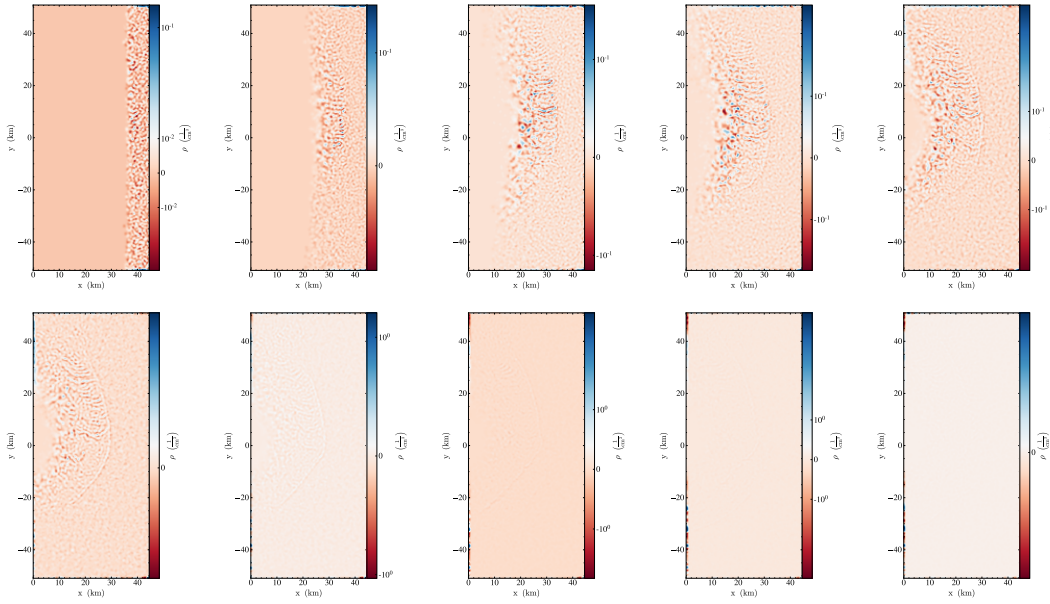


Figure 4.3 Net number density (prton density - electron density)

approximately  $14 \text{ cm}^{-3}$ , 12.4 times the solar wind value. The narrow boundary of the mini-magnetosphere is not smooth due to waves, turbulence, and instabilities . The density varies both towards the surface and parallel to the surface. In regions between magnetic cusps, both electron and proton have their lowest density and the surface is well shielded from the solar wind. No bow shock structure similar to the earth's bow shock is observed, this may be attributed to the small length scale of the interaction region compared with the gyro-radii of the ions Kallio et al. (2012). Particles' speeds are high enough before their motion are significantly modified by the halo region and the dipole magnetic field, so no stationary shock can exist.

Only the electron population is effectively magnetized in the vast region of the simulation box, whereas the ions are only magnetized near the lunar surface, give the gyro-radii of the electrons and protons at the halo location are 300 m and 100 km. The ions could easily penetrate the density halo and create a charge separation with the electrons. This separation, in turn, creates a large electric field. This electric field's main direction lies in the x-z plane (see Figure 4.4, 4.5, 4.6). The large normal electric field with the magnitude of 100 mV/m exist to decelerate ions and accelerate electrons. Also the large electric fields in the cusp regions perpendicular to the solar wind flow acts to deflect the charged particles motion towards the cusp regions. Because in theory (Bamford et al., 2012), the electric field is proportional to the gradient in the magnetic field intensity, the particles scattering can be seen to be omnidirectionally pointing outward,

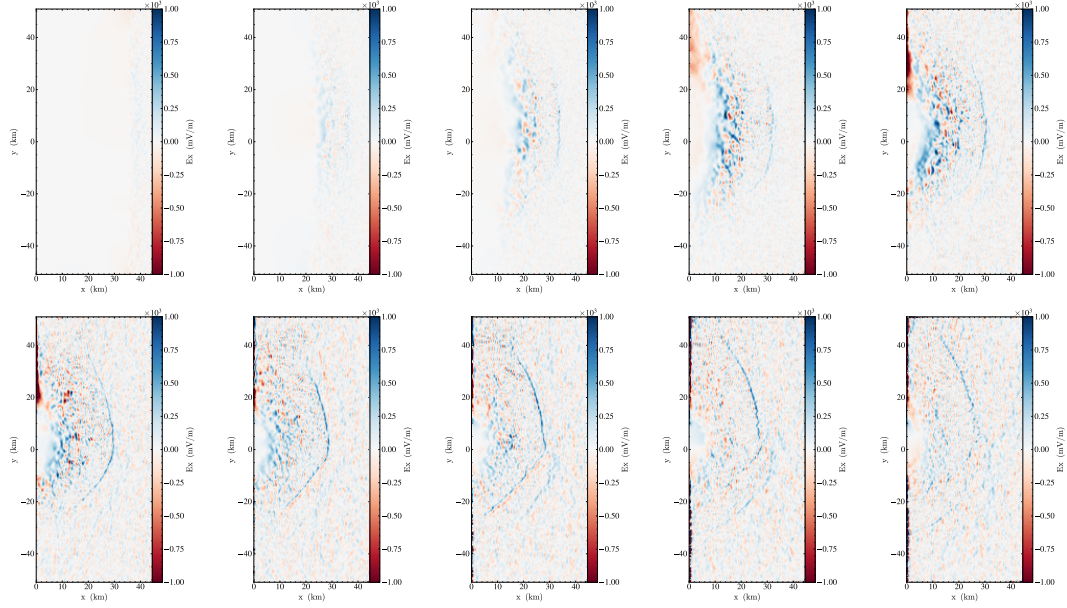


Figure 4.4 Electric field in direction x

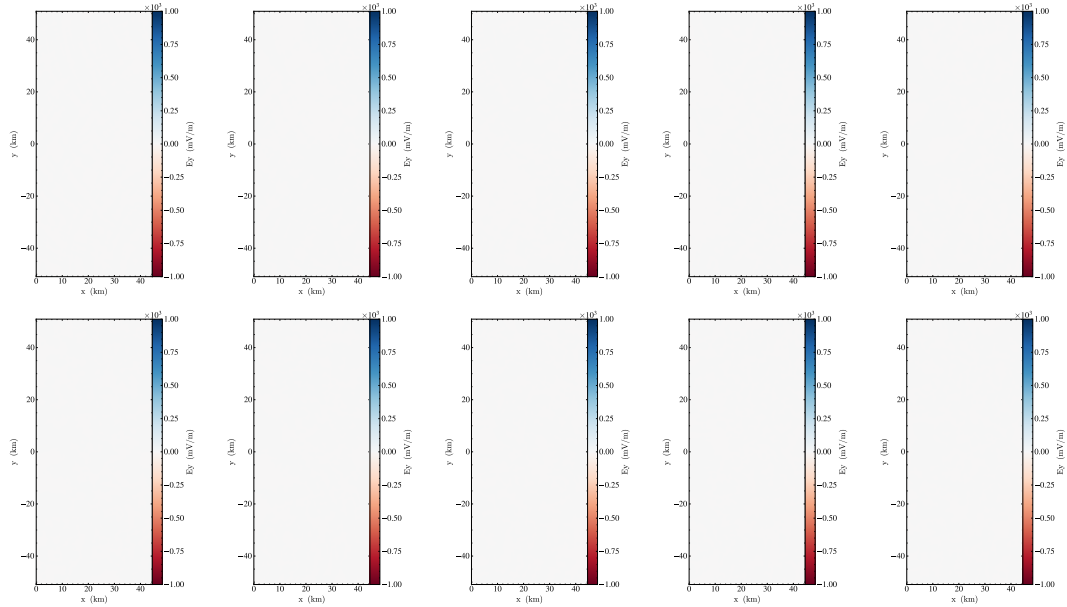


Figure 4.5 Electric field in direction y

regardless of the magnetic field orientation. In conclusion, the formation of the mini-magnetosphere is mainly an electrostatic effect due to the charge separation. Note this magnitude of 100 mV/m is larger than the values obtained by Deca et al. (2015) (75 mV/m), but since they use an ion-to-electron mass ratio of  $m_i/m_e = 256$ , lower values in their model are to be expected.

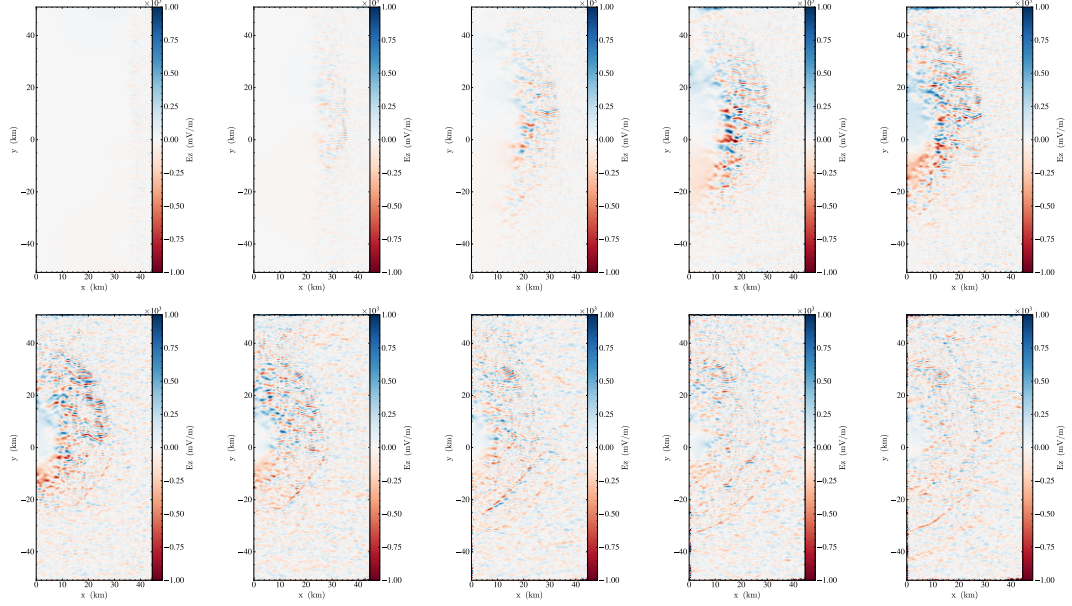


Figure 4.6 Electric field in direction z

### 4.3 Proton and Electron dynamics

Both the electron and proton population is significantly heated in directions perpendicular to the dipole axis. The electron population is accelerated in the -Z direction while However, no statistical desperation from initial can be observed in directions parallel to the dipole moment from Figure.

The electron population is accelerated in the -Z direction near the lunar surface and the proton population is accelerated in the +Z direction. Deca et al. (2015) evaluate the effects of the magnetic  $\nabla B +$  curvature drift  $v_B$  and the electric drift  $v_E$ . The electric field drift is prevalent by an order of magnitude for the electron population, thus formally dominating an overall motion of the electrons in the electrosheath toward the -Z direction. On the other side, the much heavier protons' flow speed  $v_{sw}$  much larger than their velocity speed  $v_{th,i}$ . The magnetic drift component surpass the electric field drift in this case.

$$\mathbf{v}_B = \frac{mv_{\perp}^2}{2eB^3}(\mathbf{B} \times \nabla B) + \frac{mv_{\parallel}^2}{eR_C^2B^2}(\mathbf{R}_c \times \mathbf{B})$$

$$\mathbf{v}_E = \left(1 + \frac{1}{4}r_s^2\nabla^2\right) \frac{\mathbf{E} \times \mathbf{B}}{B^2}$$

One interesting thing to notice in our simulation is that the when the plasma is far away from the lunar surface electrons population is accelerated in the +Z direction,

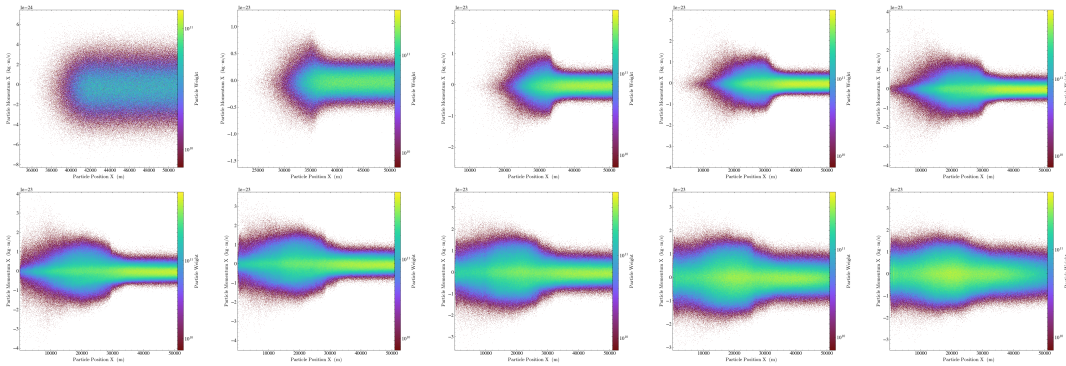


Figure 4.7 Electron momentum in direction x

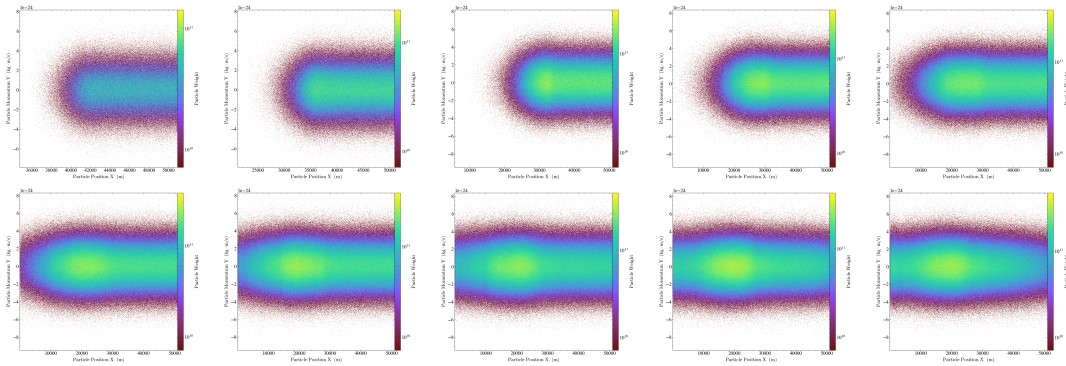


Figure 4.8 Electron momentum in direction x

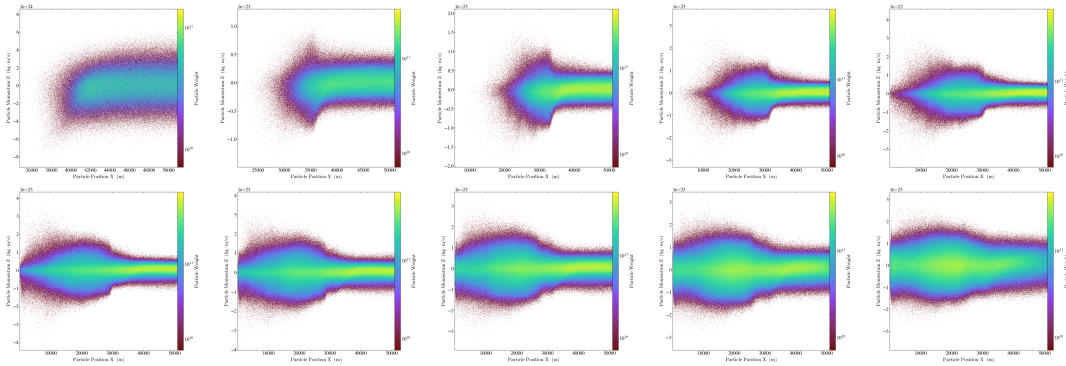


Figure 4.9 Electron momentum in direction x

whereas the proton has no corresponding acceleration (see Figure 4.15 4.16). The interplanetary magnetic field may be the possible cause for this strange phenomena as the electrons are magnetized even in the weak IMF field. However, other mechanisms like anisotropic heating may also attribute to the modified velocity distribution. The detailed reason needs further examination and a parametric study about the direction and magnitude of the IMF magnetic fields can help provide insight into this.

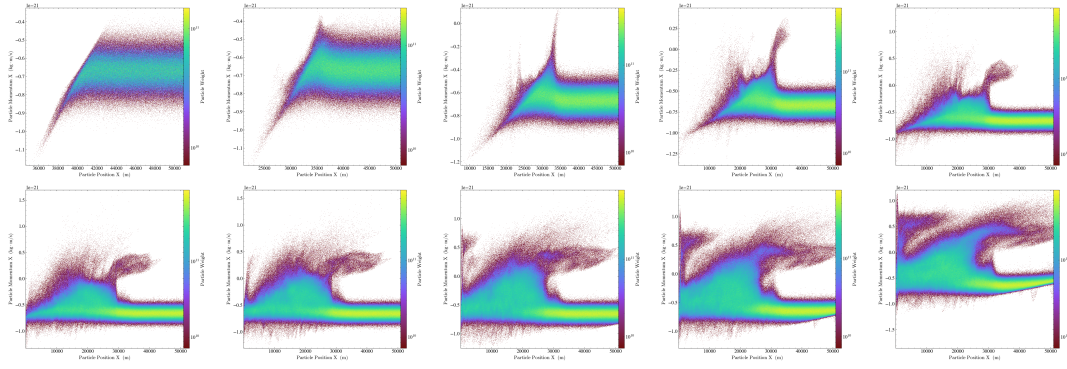


Figure 4.10 Proton momentum in direction x

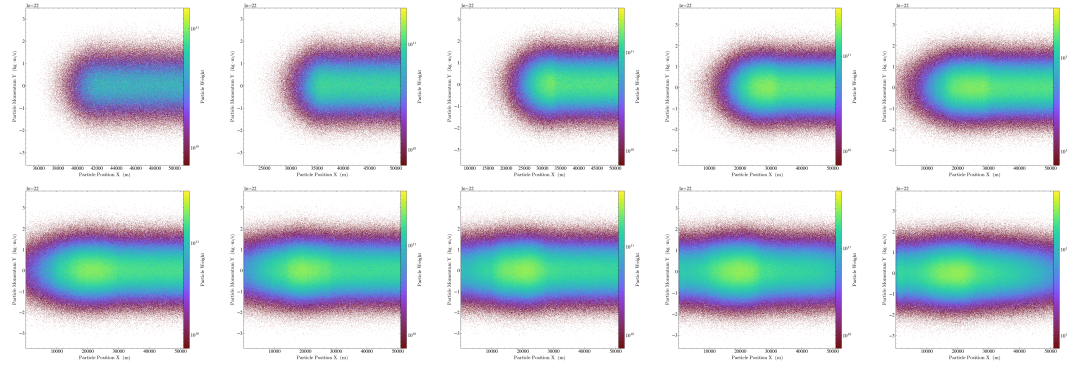


Figure 4.11 Proton momentum in direction x

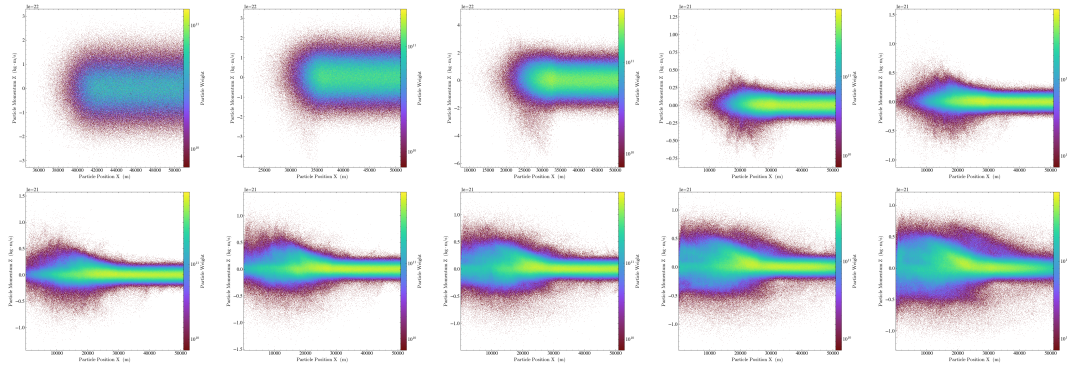


Figure 4.12 Proton momentum in direction x

#### 4.4 Parametric analysis

In the last part, we perform comparative experiments to study: (a) the individual influence of surface and dipole, (b) the evolution time scale, (c) numerical setting and algorithm effect on the simulation. These experiments do not extend to explore all the parameter space: they are carried out essentially to determine the important physical processes of the interaction between the solar wind and lunar magnetic anomalies. Deca et al. (2015) discuss the influence of both the IMF and solar wind direction/strength on the macroscopic structure of the minimagnetosphere with a particular focus on how the shielding efficiency changes with changing solar wind conditions. And they conclude

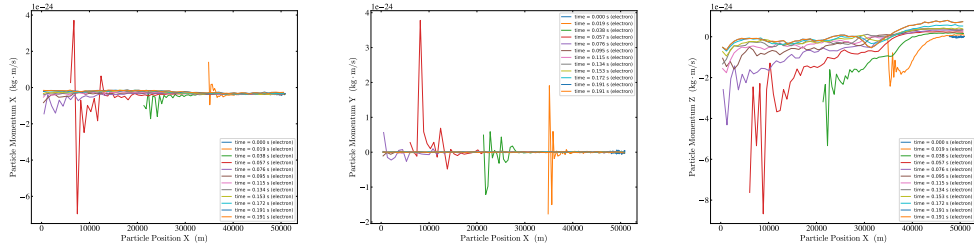


Figure 4.13 Averaged electron momentum (x,y,z direction) vs time plot

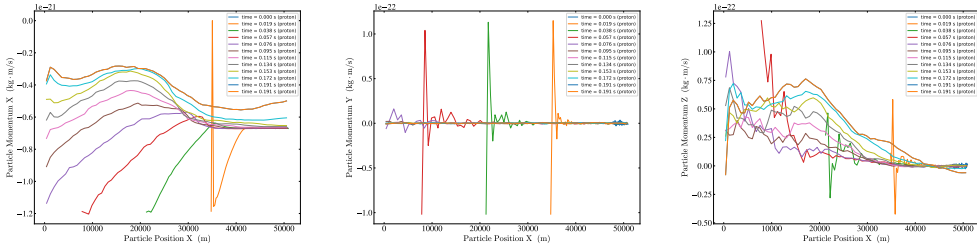


Figure 4.14 Averaged proton momentum (x,y,z direction) vs time plot

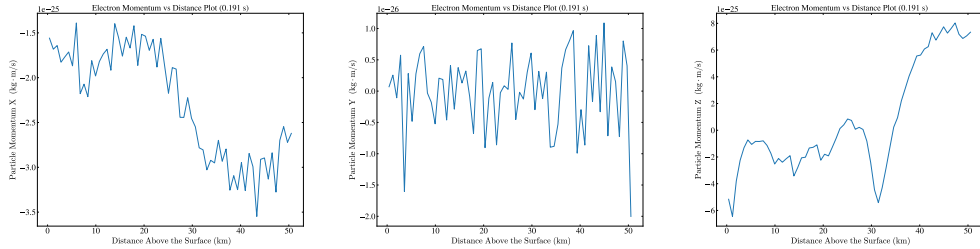


Figure 4.15 Averaged electron momentum (x,y,z direction) plot (zoom into the last timestep)

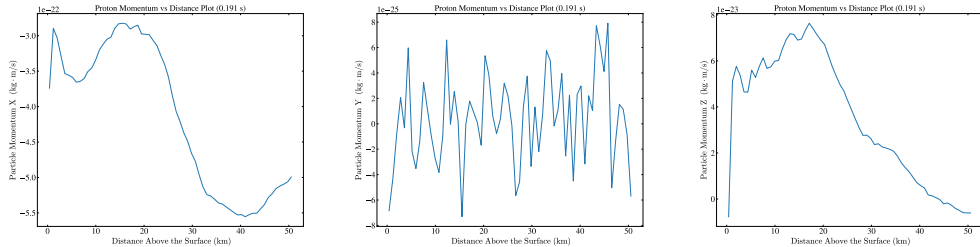


Figure 4.16 Averaged proton momentum (x,y,z direction) plot (zoom into the last timestep)

that the solar wind-LMA interaction are highly dependent on the features of the lunar and upstream plasma environment. Similar to Deca's work, Bamford et al. (2016) have analyzed parametrically the influence of the magnetic dipole configuration and the solar wind plasma Alfvén Mach parameter. We expect similar results can also be obtained, varying the magnetic dipole and environmental plasma. And benefiting from the advances in computation power and parallel algorithm (Zhang et al., 2019), Zhang et al. (2021), conducting parametric analysis is much more feasible and cheaper than the past.

#### 4.4.1 The influence of the lunar surface and the magnetic dipole

The whole interaction is determined among three components: the solar wind, the lunar surface and the magnetic dipole buried underneath. Past studies (Deca et al., 2015), Bamford et al. (2016) couple the dipole and the lunar surface. However, they have different role when acting on the solar wind: the magnetic dipole is responsible for changing charged particles motion; the lunar surface, on the other hand, absorbs the impacting particles. Both of them can modify the particle phase distribution and therefore influence the whole interaction picture. The magnetic field of the dipole bring continuous changes in the particles phase space across the area; in contrast, the lunar surface introduce abrupt breaks in the particles distribution. The abrupt change is very important for the near surface area, but is hard for the simulation to capture reasonably (more details can be found in the Appendix A).

We perform three experiments: one with both the lunar surface and magnetic dipole, one without the magnetic dipole, one without the absorbing surface, keeping the solar wind parameters and all numerical setting unchanged. The result of the one without the the magnetic dipole is quite boring. Plasma just flow through nearly all the simulation box unchanged, only small deviations can be absorbed at the boundary cells. For the remaining two experiments, we find that although a mini-magnetosphere structure emerge in both case, the case without lunar surface exhibits a more obvious asymmetry both in the space and between the particle population. The near lunar surface micro-structure and surface effects is the subject of future work.

#### 4.4.2 The evolution time scale of the solar wind-Moon interaction

Changing the duration of the simulation (see Figure 4.18), we find the overall picture remains almost identical throughout time after the mini-magnetosphere is formed. And the formation time for the mini-magnetosphere is within the order of seconds. This result is encouraging for future simulations because it means that we do not have to include the time accumulation effect of the interaction as the Moon rotates around the Earth and the Sun. Though the Moon will encounter plasma of different regimes impacting the lunar surface with various angles, we can safely assure ourselves that the simulations will give reasonable and comparable results under time fixed settings.

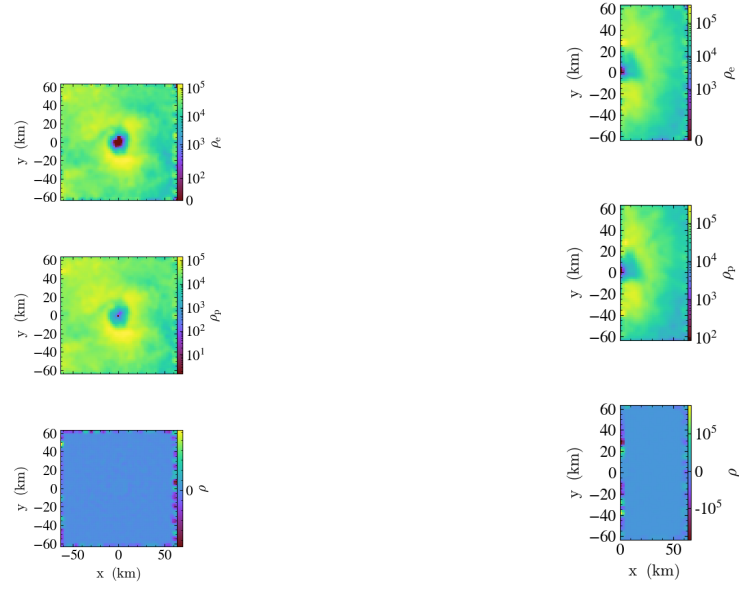


Figure 4.17 Influence of the lunar surface and the magnetic dipole

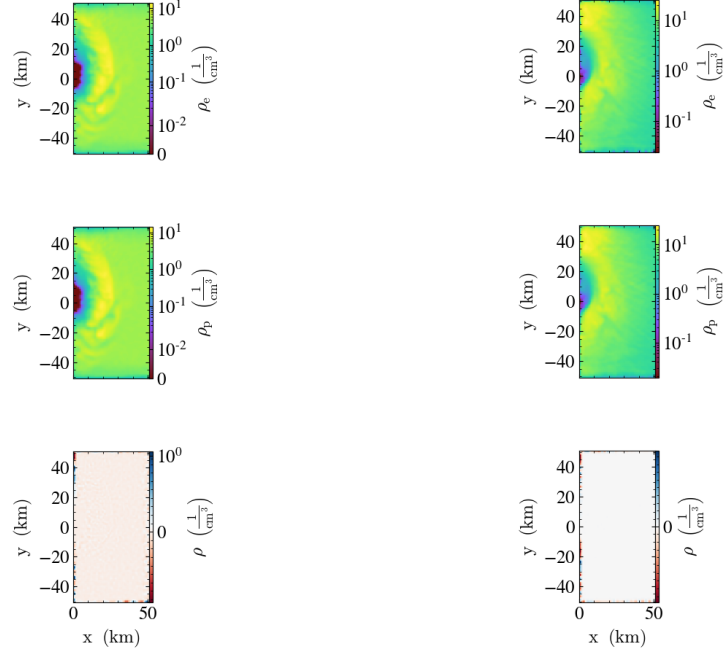


Figure 4.18 Density evolution at 1.5 and 3.5 times the solar wind flow time

#### 4.4.3 Numerical effect on the simulation

Lastly we provides results with different numerical parameters, including the number of cells, the number of particles in one cell and the particle shape in PIC algorithms. We find that the spatial resolution is the most important factor to successfully simulate the mini-magnetosphere structure. No obvious changes happen in the general interaction although a higher number of particles in one cell and a higher-order of the shape factors (splines) for the macro-particles can undoubtedly improve the simulation accu-

racy. The computation cost accompanied with the improvements, however, is a tradeoff one has to consider when performing simulation.

## Chapter 5 Summary and conclusion

We have presented in detail two-dimensional realistic kinetic simulations of the solar wind interaction with lunar crustal magnetic anomalies (three-dimensional simulation with higher space and time resolution is still running on supercomputers when the authors write the paper, but a coarse 3D simulation has exhibited a similar structure to the 2D simulation). With the WarpX particle in cell code, we identified the mini-magnetosphere structure, and confirmed that LMAs may indeed be strong enough to stand off the solar wind from directly striking the lunar surface under typical solar wind conditions. Using a dipole model centered just below an absorbing surface representing the lunar surface under open boundary conditions, we described the interaction of the solar wind with an idealized LMA. The electron population is effectively magnetized throughout the whole simulation area, while the proton population is only magnetized when they become close to the magnetic dipole. And it is the charge separation due to the mass difference between the plasma species that sets up an electric field responsible for accelerating electrons and decelerating protons.

### 5.1 Future work

At various points in the simulation and analysis, one can make sidesteps and investigate further, e.g. to incorporate more physics processes like the effects of solar illumination and associated photoemission electrons, to set a pragmatic magnetic configuration and boundary topologies (Zimmerman et al., 2015), to study the evolution of the mini-magnetosphere throughout the days and study plasma instabilities and wave-particle interactions.

Note finally, that understanding LMAs and mini-magnetospheres is not only important for Lunar science. Mars are also found to have only crustal magnetization without a global magnetic field. Similarly, Ganymede's magnetosphere formed inside the Jovian magnetosphere is considered a type of mini-magnetosphere. Simulating their interactions with the solar wind is within reach of our simulation work.

## Bibliography

- BAMFORD R A, KELLETT B, BRADFORD W J, et al. 2012. Minimagnetospheres above the Lunar Surface and the Formation of Lunar Swirls[J/OL]. *Physical Review Letters*, 109(8): 081101[2022-05-13]. <https://link.aps.org/doi/10.1103/PhysRevLett.109.081101>.
- BAMFORD R A, ALVES E P, CRUZ F, et al. 2016. 3D PIC SIMULATIONS OF COLLISIONLESS SHOCKS AT LUNAR MAGNETIC ANOMALIES AND THEIR ROLE IN FORMING LUNAR SWIRLS[J/OL]. *The Astrophysical Journal*, 830(2): 146[2022-05-13]. <https://doi.org/10.3847/0004-637x/830/2/146>. DOI: 10.3847/0004-637X/830/2/146.
- BARABASH S. 2012. Classes of the solar wind interactions in the solar system[J/OL]. *Earth, Planets and Space*, 64(2): 57-59[2022-05-12]. <https://link.springer.com/article/10.5047/eps.2012.01.005>.
- BIRDSALL C K, LANGDON A B. 1985. *Plasma Physics Via Computer Simulation* [M]. McGraw-Hill.
- DECA J, DIVIN A, LAPENTA G, et al. 2014. Electromagnetic Particle-in-Cell Simulations of the Solar Wind Interaction with Lunar Magnetic Anomalies[J/OL]. *Physical Review Letters*, 112(15): 151102[2022-01-05]. <https://link.aps.org/doi/10.1103/PhysRevLett.112.151102>.
- DECA J, POPPE A R, DIVIN A, et al. 2021. The Plasma Environment Surrounding the Reiner Gamma Magnetic Anomaly[J/OL]. *Journal of Geophysical Research: Space Physics*, 126(9): e2021JA029180[2022-01-19]. <https://onlinelibrary.wiley.com/doi/abs/10.1029/2021JA029180>.
- DECA J, DIVIN A, LEMBÈGE B, et al. 2015. General mechanism and dynamics of the solar wind interaction with lunar magnetic anomalies from 3-D particle-in-cell simulations[J/OL]. *Journal of Geophysical Research: Space Physics*, 120(8): 6443-6463[2022-01-05]. <https://onlinelibrary.wiley.com/doi/abs/10.1002/2015JA021070>.
- DECA J, DIVIN A, WANG X, et al. 2016. Three-dimensional full-kinetic simulation of the solar wind interaction with a vertical dipolar lunar magnetic anomaly[J/OL].

- Geophysical Research Letters, 43(9): 4136-4144[2022-01-19]. <https://onlinelibrary.wiley.com/doi/abs/10.1002/2016GL068535>.
- DEROUILLAT J, BECK A, PéREZ F, et al. 2018. Smilei : A collaborative, open-source, multi-purpose particle-in-cell code for plasma simulation[J/OL]. Computer Physics Communications, 222: 351-373[2021-12-16]. <https://www.sciencedirect.com/science/article/pii/S0010465517303314>. DOI: 10.1016/j.cpc.2017.09.024.
- DYADECHKIN S, KALLIO E, WURZ P. 2015. New fully kinetic model for the study of electric potential, plasma, and dust above lunar landscapes[J/OL]. Journal of Geophysical Research: Space Physics, 120(3): 1589-1606[2022-05-13]. <https://onlinelibrary.wiley.com/doi/abs/10.1002/2014JA020511>.
- FATEMI S, HOLMSTRÖM M, FUTAANA Y, et al. 2014. Effects of protons reflected by lunar crustal magnetic fields on the global lunar plasma environment[J/OL]. Journal of Geophysical Research: Space Physics, 119(8): 6095-6105[2022-05-12]. <https://onlinelibrary.wiley.com/doi/abs/10.1002/2014JA019900>.
- FEUERBACHER B, ANDEREGG M, FITTON B, et al. 1972. Photoemission from lunar surface fines and the lunar photoelectron sheath[J/OL]. Lunar and Planetary Science Conference Proceedings, 3: 2655[2022-05-24]. <https://ui.adsabs.harvard.edu/abs/1972LPSC....3.2655F>.
- GARRICK-BETHELL I, HEAD J W, PIETERS C M. 2011. Spectral properties, magnetic fields, and dust transport at lunar swirls[J/OL]. Icarus, 212(2): 480-492 [2022-05-23]. <https://linkinghub.elsevier.com/retrieve/pii/S0019103510004550>. DOI: 10.1016/j.icarus.2010.11.036.
- HALEKAS J S, POPPE A, DELORY G T, et al. 2012. Solar wind electron interaction with the dayside lunar surface and crustal magnetic fields: Evidence for precursor effects[J/OL]. Earth, Planets and Space, 64(2): 73-82[2022-01-20]. <https://link.springer.com/article/10.5047/eps.2011.03.008>.
- HARADA Y, HALEKAS J S. 2016. Upstream Waves and Particles at the Moon [M/OL]//Low-Frequency Waves in Space Plasmas. American Geophysical Union (AGU): 307-322[2022-01-20]. <https://onlinelibrary.wiley.com/doi/abs/10.1002/9781119055006.ch18>.
- HARADA Y. 2015. Springer Theses: Interactions of Earth's Magnetotail Plasma with the Surface, Plasma, and Magnetic Anomalies of the Moon[M/OL]. Tokyo:

- Springer Japan[2022-05-12]. <http://link.springer.com/10.1007/978-4-431-55084-6>.
- HOOD L L. 2021b. Lunar Magnetic Anomalies[J/OL]. Encyclopedia of Lunar Science: 1-9[2022-04-29]. [https://link.springer.com/referenceworkentry/10.1007/978-3-319-05546-6\\_4-3](https://link.springer.com/referenceworkentry/10.1007/978-3-319-05546-6_4-3).
- HOOD L L, TORRES C B, OLIVEIRA J S, et al. 2021a. A New Large-Scale Map of the Lunar Crustal Magnetic Field and Its Interpretation[J/OL]. Journal of Geophysical Research: Planets, 126(2): e2020JE006667[2022-05-12]. <https://onlinelibrary.wiley.com/doi/abs/10.1029/2020JE006667>.
- JARVINEN R, ALHO M, KALLIO E, et al. 2014. On vertical electric fields at lunar magnetic anomalies[J/OL]. Geophysical Research Letters, 41(7): 2243-2249 [2022-05-13]. <https://onlinelibrary.wiley.com/doi/abs/10.1002/2014GL059788>.
- KALLIO E, JARVINEN R, DYADECHKIN S, et al. 2012. Kinetic simulations of finite gyroradius effects in the lunar plasma environment on global, meso, and microscales[J/OL]. Planetary and Space Science, 74(1): 146-155[2022-01-05]. <https://www.sciencedirect.com/science/article/pii/S0032063312002875>. DOI: 10.1016/j.pss.2012.09.012.
- KURATA M, TSUNAKAWA H, SAITO Y, et al. 2005. Mini-magnetosphere over the Reiner Gamma magnetic anomaly region on the Moon[J/OL]. Geophysical Research Letters, 32(24)[2022-01-11]. <https://onlinelibrary.wiley.com/doi/abs/10.1029/2005GL024097>.
- LAPENTA G, BRACKBILL J U. 1996. Contact discontinuities in collisionless plasmas: A comparison of hybrid and kinetic simulations[J/OL]. Geophysical Research Letters, 23(14): 1713-1716[2022-05-17]. <https://onlinelibrary.wiley.com/doi/abs/10.1029/96GL01845>.
- LIN R P, MITCHELL D L, CURTIS D W, et al. 1998. Lunar Surface Magnetic Fields and Their Interaction with the Solar Wind: Results from Lunar Prospector[J/OL]. Science, 281(5382): 1480-1484[2022-05-22]. <https://www.science.org/doi/10.1126/science.281.5382.1480>.
- LUE C, FUTAANA Y, BARABASH S, et al. 2011. Strong influence of lunar crustal fields on the solar wind flow[J/OL]. Geophysical Research Letters, 38(3)[2022-02-25]. <https://onlinelibrary.wiley.com/doi/abs/10.1029/2010GL046215>.

- MARKIDIS S, LAPENTA G, Rizwan-uddin. 2010. Multi-scale simulations of plasma with iPIC3D[J/OL]. *Mathematics and Computers in Simulation*, 80(7): 1509-1519 [2021-11-12]. <https://www.sciencedirect.com/science/article/pii/S0378475409002444>. DOI: 10.1016/j.matcom.2009.08.038.
- MITCHELL D L, HALEKAS J S, LIN R P, et al. 2008. Global mapping of lunar crustal magnetic fields by Lunar Prospector[J/OL]. *Icarus*, 194(2): 401-409[2022-01-11]. <https://www.sciencedirect.com/science/article/pii/S0019103507005829>. DOI: 10.1016/j.icarus.2007.10.027.
- NAKAGAWA T, TAKAHASHI Y, IIZIMA M. 2003. GEOTAIL observation of upstream ULF waves associated with lunar wake[J/OL]. *Earth, Planets and Space*, 55(9): 569-580[2022-05-18]. <https://doi.org/10.1186/BF03351789>.
- NASA. 2018. NASA Strategic Plan 2018[Z].
- NASA. 2020. NASA's Lunar Exploration Program Overview[M/OL]. National Aeronautics and Space Administration. [https://www.nasa.gov/sites/default/files/atoms/files/artemis\\_plan-20200921.pdf](https://www.nasa.gov/sites/default/files/atoms/files/artemis_plan-20200921.pdf).
- NESS N F, BEHANNON K W, SCEARCE C S, et al. 1967. Early results from the magnetic field experiment on lunar Explorer 35[J/OL]. *Journal of Geophysical Research (1896-1977)*, 72(23): 5769-5778[2022-05-18]. <https://onlinelibrary.wiley.com/doi/abs/10.1029/JZ072i023p05769>.
- NISHINO M N, FUJIMOTO M, MAEZAWA K, et al. 2009. Solar-wind proton access deep into the near-Moon wake[J/OL]. *Geophysical Research Letters*, 36(16)[2022-05-18]. <https://onlinelibrary.wiley.com/doi/abs/10.1029/2009GL039444>.
- OWENS M J. 2020. Solar-Wind Structure[M/OL]//Oxford Research Encyclopedia of Physics. Oxford University Press[2022-05-20]. <https://oxfordre.com/physics/view/10.1093/acrefore/9780190871994.001.0001/acrefore-9780190871994-e-19>. DOI: 10.1093/acrefore/9780190871994.013.19.
- PING J, MENG Z. 2017. Lunar Surface, Electrical Conductivity[M/OL]//CUDNIK B. Encyclopedia of Lunar Science. Cham: Springer International Publishing: 1-3 [2022-05-18]. [https://doi.org/10.1007/978-3-319-05546-6\\_67-1](https://doi.org/10.1007/978-3-319-05546-6_67-1).
- POPPE A R, HALEKAS J S, DELORY G T, et al. 2012. Particle-in-cell simulations of the solar wind interaction with lunar crustal magnetic anomalies: Magnetic cusp regions[J/OL]. *Journal of Geophysical Research: Space Physics*, 117(A9)[2022-05-18]. <https://doi.org/10.1029/2011JA017050>. DOI: 10.1029/2011JA017050.

- 01-11]. <https://onlinelibrary.wiley.com/doi/abs/10.1029/2012JA017844>.
- POPPE A, HORÁNYI M. 2010. Simulations of the photoelectron sheath and dust levitation on the lunar surface[J/OL]. *Journal of Geophysical Research: Space Physics*, 115(A8)[2021-11-19]. <https://onlinelibrary.wiley.com/doi/abs/10.1029/2010JA015286>.
- SAITO Y, YOKOTA S, ASAMURA K, et al. 2010. In-flight Performance and Initial Results of Plasma Energy Angle and Composition Experiment (PACE) on SELENE (Kaguya)[J/OL]. *Space Science Reviews*, 154(1): 265-303[2022-05-06]. <https://doi.org/10.1007/s11214-010-9647-x>.
- SAITO Y, NISHINO M N, FUJIMOTO M, et al. 2012. Simultaneous observation of the electron acceleration and ion deceleration over lunar magnetic anomalies[J/OL]. *Earth, Planets and Space*, 64(2): 4[2022-01-05]. <https://doi.org/10.5047/eps.2011.07.011>.
- TAFLOVE A, HAGNESS S C, PIKET-MAY M. 2005. 9 - Computational Electromagnetics: The Finite-Difference Time-Domain Method[M/OL]//CHEN W K. *The Electrical Engineering Handbook*. Burlington: Academic Press: 629-670[2022-03-27]. <https://www.sciencedirect.com/science/article/pii/B9780121709600500463>. DOI: 10.1016/B978-012170960-0/50046-3.
- TAKAHASHI F, TSUNAKAWA H, SHIMIZU H, et al. 2014. Reorientation of the early lunar pole[J/OL]. *Nature Geoscience*, 7(6): 409-412[2022-05-17]. <https://www.nature.com/articles/ngeo2150>. DOI: 10.1038/ngeo2150.
- TSUNAKAWA H, TAKAHASHI F, SHIMIZU H, et al. 2015. Surface vector mapping of magnetic anomalies over the Moon using Kaguya and Lunar Prospector observations[J/OL]. *Journal of Geophysical Research: Planets*, 120(6): 1160-1185 [2022-04-10]. <https://onlinelibrary.wiley.com/doi/abs/10.1002/2014JE004785>.
- VAY J L. 2008. Simulation of beams or plasmas crossing at relativistic velocity[J/OL]. *Physics of Plasmas*, 15(5): 056701[2022-05-24]. <http://aip.scitation.org/doi/10.1063/1.2837054>.
- VAY J L, ALMGREN A, BELL J, et al. 2017. Warp-X: A new exascale computing platform for beam-plasma simulations[Z].
- VAY J L, ALMGREN A, BELL J, et al. 2018. Warp-X: A new exascale computing platform for beam-plasma simulations[J/OL]. *Nuclear Instruments and Methods*

- in Physics Research Section A: Accelerators, Spectrometers, Detectors and Associated Equipment, 909: 476-479[2022-03-23]. <https://www.sciencedirect.com/science/article/pii/S0168900218300524>. DOI: 10.1016/j.nima.2018.01.035.
- VERBONCOEUR J P. 2005. Particle simulation of plasmas: review and advances [J/OL]. Plasma Physics and Controlled Fusion, 47(5A): A231-A260[2021-08-04]. <https://doi.org/10.1088/0741-3335/47/5a/017>. DOI: 10.1088/0741-3335/47/5A/017.
- VORBURGER A, WURZ P, BARABASH S, et al. 2013. Energetic neutral atom imaging of the lunar surface[J/OL]. Journal of Geophysical Research: Space Physics, 118(7): 3937-3945[2022-05-23]. <https://onlinelibrary.wiley.com/doi/abs/10.1002/jgra.50337>.
- WHANG Y C. 1968. Theoretical Study of the Magnetic Field in the Lunar Wake[J/OL]. The Physics of Fluids, 11(8): 1713-1719[2022-05-18]. <https://aip.scitation.org/doi/10.1063/1.1692185>.
- WHIPPLE E C. 1981. Potentials of surfaces in space[J/OL]. Reports on Progress in Physics, 44(11): 1197-1250[2022-05-18]. <https://doi.org/10.1088/0034-4885/44/11/002>.
- WIESER M, BARABASH S, FUTAANA Y, et al. 2010. First observation of a mini-magnetosphere above a lunar magnetic anomaly using energetic neutral atoms [J/OL]. Geophysical Research Letters, 37(5)[2022-05-16]. <https://onlinelibrary.wiley.com/doi/abs/10.1029/2009GL041721>.
- WINSKE D, YIN L, OMIDI N, et al. 2003. Hybrid Simulation Codes: Past, Present and Future—A Tutorial[J/OL]. Space Plasma Simulation: 136-165[2022-05-16]. [https://link.springer.com/chapter/10.1007/3-540-36530-3\\_8](https://link.springer.com/chapter/10.1007/3-540-36530-3_8).
- ZHANG W, ALMGREN A, BECKNER V, et al. 2019. AMReX: a framework for block-structured adaptive mesh refinement[J/OL]. Journal of Open Source Software, 4 (37): 1370[2022-01-26]. <https://joss.theoj.org/papers/10.21105/joss.01370>. DOI: 10/ghr39d.
- ZHANG W, MYERS A, GOTTL K, et al. 2021. AMReX: Block-structured adaptive mesh refinement for multiphysics applications[J/OL]. The International Journal of High Performance Computing Applications, 35(6): 508-526[2022-05-23]. <https://doi.org/10.1177/10943420211022811>.

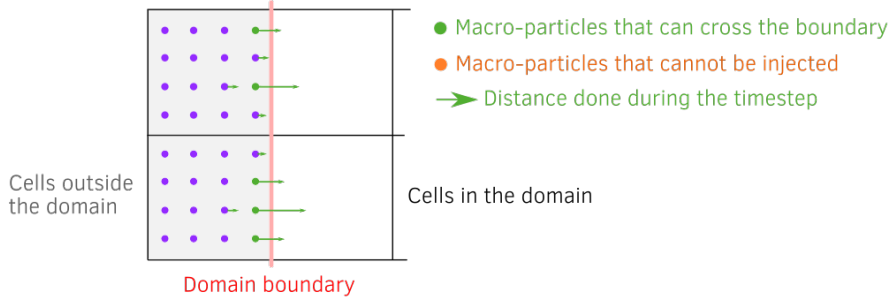
ZIMMERMAN M I, FARRELL W M, POPPE A R. 2015. Kinetic simulations of kilometer-scale mini-magnetosphere formation on the Moon[J/OL]. Journal of Geophysical Research: Planets, 120(11): 1893-1903[2022-04-09]. <https://onlinelibrary.wiley.com/doi/abs/10.1002/2015JE004865>.

## Appendix A Techinal caveats

### A.1 Particle injection

Injecting particles can be a tricky thing in numerical implementation. Currently we find three available approaches to do this and every approach provide some choices to tune the simulation. First and the simplest way is to not use injection at all: extend the simulation length, so that in a small simulation area we have continuous plasma flow through it. The second method is to initialize macro-particles in the cells behind the boundaries (outside the simulation domain). And in the PIC loop structure, the particle injection occurs after current projection on the grid, particle sorting and synchronizations. Injected macro-particles therefore do not contribute to the current and fields of the current iteration but they are taken into account in the diagnostics. This method is adopted in Smilei (Derouillat et al., 2018). The third approach is the most intuitive: place a surface and inject the particles through the flux. This approach is implemented in WarpX (Vay et al., 2017). Although the first one seems to be the most computationally expensive one as it require to simulate a larger domain and keep track of all the particles, it is in fact the most fast one in modern highly paralleled computers. It only needs to generate the particles at the first time while the second and the third methods need to produce new particles at every timestep by sampling the particle distribution function. For the first method, we can use mesh refinement techniques to speed up the computation in the areas that we are not interested. If the second and third approaches is a must in the case of simulating the long time interaction or time-changing particle distributions, we recommend to inject both positively and negatively charged species at the same time to ensure a neutral plasma. And to strengthen neutrality, species may be created at the same positions. And if the particle momentum is drawn from a Maxwellian, using a random positionning instead of the regular one may be a better choice because regular positionning may induce numerical effects such as loss of charge and spurious field near the boundary. The reason is explained in the following figure A.1. The regular positionning works when injecting a drifting cold plasma with a drift velocity sufficiently high to let the particles entering the simulation domain.

Regular position: only particles with enough velocity can cross the boundary and be injected



Random position:

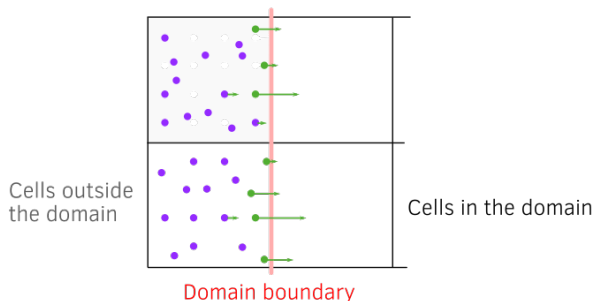


Figure A.1 Position choice (from Smilei Website)

## A.2 Particle reflection at the boundary

Even if we implement an open boundary condition, particle reflection can still occur at the boundary because of the discretization of time in numerical algorithms. As there is some randomness in positions and momentum, electrons and ions will slowly separate, thus creating random electric + magnetic field noise. When the plasma reaches the boundaries, it may happen that an electron is removed, but the ion is still in the box if the timestep is large enough to separate them. This will create a local artificial space-charge field that is later compensated by the ion leaving the box and short-lived electromagnetic noise. When particles come from far from boundary they get more separated over time, this noise becomes more and more important. As a consequence, we may reach a point where adding the noise from several particles is enough to reflect one other particle. Several ways exist to help mitigate this artificial effect like reducing temperature, using "regular spacing" to remove any randomness, staying far from boundaries to ignore the boundary effect, having many more particles or adopting a smaller timestep to reduce the noise. This most feasible way in our simulation is to use a smaller timestep by increasing the spatial resolution (number of cells). Because the Courant–Friedrichs–Lowy condition (CFL) constraint, the timestep is reduced consequently.

## Acknowledgements

This research used the open-source particle-in-cell code WarpX <https://github.com/ECP-WarpX/WarpX>, primarily funded by the US DOE Exascale Computing Project. Primary WarpX contributors are with LBNL, LLNL, CEA-LIDYL, SLAC, DESY, CERN, and Modern Electron. We acknowledge all WarpX contributors.

This research used the open-source particle-in-cell code Smilei <https://smileipic.gitub.io/Smilei/>. We acknowledge all Smilei contributors.

This research used the open-source volumetric data analyzing and visualizing tool yt <https://yt-project.org/>. We acknowledge all yt contributors.

## Acknowledgements

首先我要感谢我的导师陶鑫老师，感谢陶老师启蒙我科研的道路，在两年的时间里给予了我充分探索科研兴趣的自由，并在论文的选题到实验的实施上都给予了我莫大的反馈与帮助。感谢课题组里的吴一凡、安泽宇、蔡彬、吴泽寅师兄以及腾尚纯师姐给予我经验上的指导。

感谢科大所有的同学、老师还有后勤工作人员，四年的求学生涯里，我难忘和你们的接触与交流，难忘你们的善意。

感谢我的家人们，感谢爸爸、妈妈、奶奶还有远在天上的爷爷。你们慢慢地带我接触这个世界，让我明白生活的现实和人性的复杂时依然相信温柔相信希望，你们的爱构成了我最坚实的内核，我也爱你们。

感谢我的朋友们，俊龙、一帆、阿飘、伟豪、阿洁、超超、涵姐、邢云、嘉炜、子茗、方旭、司司，刘维。没有你们的大学生活将少了多少乐趣。感谢祝寿、可可、妈桃，愿友谊长存。感谢羽翩，你的爱让我对这世界的爱与期望又多了好多。

感谢科考，带我走过山川大漠与河海，给予我充沛的活力与热忱的渴望。感谢攀岩，让我在与自己的对抗中在身体的极限下，一次次地品味到了坚持这两字的不易与可能。感谢岩队，感谢老孟、飘飘、龙队、潘宝宝、方圆、茜茜、志远，还有那些许许多多打过保护的人，安全所托，生命所系。感谢大山感谢丛林感谢自然，感谢你们包容接纳了曾经无知无畏的我。

感谢月亮这个小妖精，你是这篇论文的研究对象，可你依旧神秘让我充满好奇，你在天上打转的时候，有没有想过地上的人正为怎么研究你发着愁呢。感谢脚下的土地，清晨的阳光，春日的微风，在疫情封闭的校园里，你们充盈了我的生活，惊喜了我的日常。

最后我想把这篇论文献给我的爷爷，在有很多星星的夜晚时，我总会突然想起你，你的善良构成了我的人生信仰。

2022年6月